Microporous and Mesoporous Materials 278 (2019) 387–396

Contents lists available at ScienceDirect

Microporous and Mesoporous Materials

journal homepage: www.elsevier.com/locate/micromeso

Fabrication of hierarchical Lewis acid Sn-BEA with tunable hydrophobicity for cellulosic sugar isomerization

Hong Je Cho[a], Nicholas S. Gould[b], Vivek Vattipalli[a], Sanket Sabnis[a], Watcharop Chaikittisilp[c,d], Tatsuya Okubo[c], Bingjun Xu[b], Wei Fan[a,*]

[a] Department of Chemical Engineering, University of Massachusetts, Amherst, MA, 01003, United States
[b] Department of Chemical and Biomolecular Engineering, University of Delaware, Newark, DE, 19716, United States
[c] Department of Chemical System Engineering, The University of Tokyo, Tokyo, 113-8656, Japan
[d] Research and Services Division of Materials Data and Integrated System (MaDIS), National Institute for Materials Science (NIMS), Ibaraki, 305-0047, Japan

ARTICLE INFO

Keywords:
Lewis acid Sn-BEA
Hierarchical zeolites
Hydrophobicity
Recrystallization
Sugar isomerization

ABSTRACT

Lewis acid Sn-BEA catalysts with tunable morphology and hydrophobicity were successfully synthesized by the recrystallization of post-synthetic Sn-BEA in the presence of ammonium fluoride (NH_4F) and tetraethylammonium bromide (TEABr). Three-dimensionally ordered mesoporous imprinted (3DOm-i) and nanocrystalline Sn-BEA catalysts with hydrophobic surface were synthesized for the first time by the method. This recrystallization method includes the dissolution of crystalline zeolite BEA by fluoride ions and the rearrangement of different types of silanol defects in the presence of TEABr. The method allows the final products to simultaneously inherit the morphology of their parent Al-BEA zeolites, and significantly reduce silanol defects within the catalysts. The Sn-BEA catalysts synthesized from the recrystallization method show largely enhanced catalytic performance for both glucose isomerization and bulky lactose isomerization in different solvents, which is presumably due to the hydrophobic surface and improved molecular transport property in the hierarchical zeolites. The recrystallization approach is a facile and reliable strategy to improve the hydrophobicity of zeolite catalysts with tunable morphologies ranging from nanocrystals to hierarchical structures.

1. Introduction

Zeolites are microporous crystalline materials with distinct pore dimension, connectivity, and composition. Due to their hydrothermal stability and molecular sieving capability, aluminosilicate zeolites have been widely used in catalysis, ion-exchange and separation [1,2]. Different from aluminosilicate zeolites, Sn, Ti and Zr-containing zeolites exhibit unique Lewis acidity in the presence of water. In particular, Sn-BEA, a stannosilicate zeolite with BEA topology, is a promising catalyst for the Baeyer-Villiger (BV) reaction [3–5], reduction of carbonyl compounds with secondary alcohols through the Meerwein-Ponndorf-Verley (MPV) reaction [3,6,7], ring-opening hydration of epoxides [8], the Diels-Alder and dehydration reactions for producing *p*-xylene from 2,5-dimethylfuran and ethylene [9–15], and isomerization of cellulosic sugars [16–22]. The unique catalytic performance of Sn-BEA in the presence of water is attributable to its Lewis acidity stemming from the tetrahedrally coordinated framework Sn and hydrophobic nature associated with a defect-free siliceous framework [18,20,23–25].

Hydrophobic Sn-BEA (denoted as Sn-BEA-HF) is conventionally synthesized in the presence of hydrofluoric acid (HF). In the synthesis route, fluoride anions act as a mineralizing agent for the crystallization, and pair with the positive charges of organic structure-directing agents (OSDAs) such as tetraethylammonium (TEA^+). Therefore, no structural defect, $Si{-}O^-$, is required to balance the positive charge of the OSDAs in the fluoride-assisted synthesis method, which results in low-defect or defect-free zeolite structures with hydrophobic surface. Although the fluoride-assisted synthesis method leads to superior hydrophobicity for the materials, several challenges need to be tackled before using them in industrial applications. The Sn-BEA-HF usually possesses a large crystal size due to limited nucleation and slow crystal growth in the presence of HF [26–28]. Mass transfer limitations caused by the large crystal size can hamper their catalytic properties, in particular, when bulky reactants and/or products are involved. In addition, the use of HF is strictly regulated because of safety requirements in a material manufacturing process.

Recently, alternative synthesis approaches such as post-synthetic methods have been developed for Sn-BEA [29–35]. Li and coworkers revealed that Sn can be grafted onto dealuminated BEA via chemical

* Corresponding author.
E-mail address: wfan@ecs.umass.edu (W. Fan).

https://doi.org/10.1016/j.micromeso.2018.12.046
Received 30 November 2018; Accepted 31 December 2018
Available online 02 January 2019
1387-1811/

vapor deposition with tin chloride ($SnCl_4$) vapor [33]. Hammond et al. reported a solid state ion-exchange (SSIE) route where tin acetate was physically mixed with dealuminated BEA followed by calcination [31,32]. Dijkmans et al. employed a solution-based approach to incorporate Sn into dealuminated BEA [34,35]. In general, these post-synthetic methods include an acid treatment to eliminate framework Al from the parent Al-containing zeolites, which creates silanol (Si—OH) nests. The reaction between Sn precursors with the silanol nests forms tetrahedrally coordinated Sn sites. In the post-synthetic approaches, the morphology of the parent aluminosilicate BEA samples can be retained during the dealumination and Sn-insertion steps under optimized synthesis conditions. Therefore, Sn-BEA catalysts with various morphologies ranging from nanocrystals to hierarchical structures have been synthesized. However, the defect density of the Sn-BEA samples synthesized by the post-synthetic approaches (denoted as Sn-BEA-PS) is much higher than the samples made via the fluoride-assisted synthesis route. This is because of the low mobility of Sn precursors and the limited control over the type and amount of silanol defects in the dealuminated BEA. Because of the high defect density and low hydrophobicity, for many reactions Sn-BEA-PS catalysts showed lower catalytic performance than hydrophobic Sn-BEA-HF even though Sn-BEA-PS catalysts possessed improved mass transport property due to their small particle size and hierarchical structure [17,30,36].

Herein, we demonstrate that morphology-tunable Sn-BEA with a low density of structural defects can be achieved by healing the silanol defects using a recrystallization method. In this method, Sn was incorporated into the dealuminated BEA with different morphologies by a post-synthetic route. The resultant materials undergo recrystallization in the presence of tetraethylammonium bromide (TEABr) and ammonium fluoride (NH_4F) using a steam-assisted crystallization (SAC) method. Bulky, 200 nm and hierarchical Sn-BEA zeolites with reduced structural defects were synthesized by this method. The catalytic properties of the synthesized Sn-BEA were systematically evaluated for the isomerization of glucose (C_6 sugar) and lactose (C_6 sugar dimer) in different solvents. We show that improved hydrophobicity is crucial for leveraging the catalytic properties of the Sn-BEA catalysts with hierarchical structures.

2. Experimental

2.1. Synthesis of Sn-BEA-HF

Sn-BEA-HF was synthesized according to the method reported by Chang and coworkers [37]. Typically, 10.47 g of tetraethylorthosilicate (TEOS, 98%, Alfa Aesar) was mixed into 11.51 g of tetraethylammonium hydroxide solution (TEAOH, 35 wt%. Alfa Aesar or SACHEM), and stirred at room temperature until it became homogeneous. To this solution, 0.15 g of tin chloride hydrate ($SnCl_4{\cdot}xH_2O$, 34.4 wt% Sn, Alfa Aesar) dissolved in 0.96 g of deionized water was added. The mixture was then stirred in a hood until ethanol generated from the hydrolysis of TEOS was completely evaporated. Then, 0.560 mL of dealuminated zeolite beta seed solution (0.224 g mL^{-1}) was added into the solution (4.1 wt% with respect to the silica content) and mixed by a plastic spatula. Finally, 0.971 mL of hydrofluoric acid (HF, 48 wt%, Alfa Aesar) was added and homogenized by using a plastic spatula. The obtained gel with a molar composition of 1 SiO_2: 0.008 SnO_2: 0.27 TEA_2O: 0.54 HF: 7.5 H_2O was then transferred into a Teflon-lined stainless steel autoclave. For crystallization, the autoclave was heated at 140 °C with a rotation of 3 rpm for 4 days. The as-made product was collected by extensive washing with deionized water and then drying in a 100 °C oven overnight. The resulting solid was calcined in a tube furnace by flowing air with a ramping rate of 1 °C min^{-1} to 550 °C for 12 h, with the aim to remove the OSDA and fluoride ions. The Si/Sn molar ratio of the final product was 126, as determined by inductively coupled plasma (ICP) analysis.

2.2. Synthesis of Sn-BEA-PS

In this study, three parent Al-BEA zeolites were prepared: (1) commercial Al-BEA (CP814E, Si/Al = 12.5, denoted as Com_Al-BEA) from Zeolyst, (2) Al-BEA with 200 nm of a particle size (denoted as 200 nm_Al-BEA) synthesized from earlier literature [39], and (3) three-dimensionally ordered mesoporous imprinted Al-BEA (denoted as 3DOm-i_Al-BEA) synthesized by a previously reported method [40]. The prepared Al-BEA zeolites were dealuminated by treatment with nitric acid (HNO_3, 70 wt%, Fisher Scientific). Typically, 0.5 g of the Al-BEA was mixed with 25 mL of HNO_3 in a Teflon-lined stainless steel autoclave which was then put into 80 °C oven for 24 h under static conditions. The dealuminated zeolite BEA (DeAl-BEA) was washed extensively with deionized water, and subsequently dried overnight at 100 °C. To prepare post-synthesized Sn-BEA (Sn-BEA-PS), solid-state incorporation was performed by grinding tin chloride hydrate ($SnCl_4{\cdot}xH_2O$, 34.4 wt% Sn, Alfa Aesar) with DeAl-BEA for 10 min in a pestle and mortar, followed by calcination in a tube furnace by flowing air with a ramping rate of 1 °C min^{-1} to 550 °C for 12 h [31]. Each Sn-BEA-PS sample via post-synthesis was named Com_Sn-BEA-PS, 200 nm_Sn-BEA-PS and 3DOm-i_Sn-BEA-PS, depending on the parent Al-BEA used. All Sn-BEA-PS zeolites possessed a Si/Sn molar ratio of 125, confirmed by ICP analysis.

2.3. Synthesis of Sn-BEA-RC

Sn-BEA-RC was synthesized by recrystallizing Sn-BEA-PS in the presence of tetraethylammonium bromide (TEABr, 98%, Alfa Aesar) and ammonium fluoride (NH_4F, 96%, Alfa Aesar). Typically, 0.1 g of Sn-BEA-PS powder was mixed with 0.189 g of TEABr and 0.034 g of NH_4F for 5 min using a pestle and mortar. The resulting solid with a molar composition of 1 SiO_2: 0.008 SnO_2: 0.54 TEABr: 0.54 NH_4F was recrystallized via steam-assisted crystallization (SAC). 0.1 mL of deionized water was dropped into a 50 mL Teflon-lined stainless steel autoclave, and a glass vial containing the resulting powder was loaded in the autoclave, to avoid direct contact between the solid and water (Fig. S1). Subsequently, the autoclave was placed in an oven set at 170 °C, and then heated for 1 day. After recrystallization, the as-made sample was washed by centrifugation with deionized water and dried at 90 °C overnight. The dried sample was calcined in a tube furnace by flowing air with a ramping rate of 1 °C min^{-1} to 550 °C for 12 h. Each Sn-BEA-RC sample prepared by recrystallization was denoted as Com_Sn-BEA-RC, 200 nm_Sn-BEA-RC and 3DOm-i_Sn-BEA-RC, depending on the parent Al-BEA used. All Sn-BEA-RC zeolites possessed a Si/Sn molar ratio of 125, confirmed by ICP analysis.

2.4. Synthesis of Si-BEA-HF

The synthesis of Si-BEA-HF was based on a method previously published by Tong and coworkers [38]. Typically, 10.1 g of TEAOH (35% solution in water, Alfa Aesar or SACHEM) was mixed with 10.0 g of TEOS in the PTFE liner of an autoclave. This mixture was stirred vigorously overnight allowing for ethanol and some water to evaporate. Subsequently, the liner containing the mixture was placed in an 80 °C oven to allow for further evaporation until the total weight loss from the start was 13.4 g. The target H_2O to Si molar ratio after drying is 0.30. The solid was ground to a fine powder and 0.98 g of HF (48% solution in water) was added to it followed by homogenization of the mixture using a plastic spatula. The final mixture composition was 1.0 SiO_2: 0.50 HF: 0.50 TEAOH: 1.1 H_2O. The autoclave was sealed and placed in a 150 °C oven for 7 days. The washing and calcination procedures were the same as that for Sn-BEA-HF.

2.5. Material characterization

Powder X-ray diffraction (XRD) patterns of the samples were

measured on an XRD diffractometer (X'Pert Pro, PANalytical) using Cu Kα radiation generated at 45 kV and 40 mA in a 2θ range of 4–40°. A scanning electron microscope (SEM, Magellan 400, FEI) was used to investigate the morphology of the zeolites, and the samples were coated with platinum/palladium alloy prior to observation. Elemental analysis was performed on inductively coupled plasma optical emission spectroscopy (ICP-OES, iCap 6500 Dual view, Thermo Scientific). Nitrogen adsorption-desorption isotherms were measured at 77 K on an automated gas sorption analyzer (Autosorb iQ2, Quantachrome) after the samples were degassed at 300 °C under vacuum. Lewis acidity of Sn-BEA zeolites were confirmed by Fourier transform infrared (FT-IR) on an Agilent Cary 660 FT-IR Spectrometer equipped with a MCT detector (128 scans at a spectral resolution of 2 cm^{-1}). Typically, zeolite sample was loaded on a sample cell, followed by annealing at 450 °C for 1 h under vacuum of 0.01 mTorr to completely remove adsorbed water from the sample. After cooling down to 30 °C, the dehydrated solid was saturated with pyridine (99.8%, Sigma-Aldrich) or deuterated acetonitrile (CD_3CN, 99.8%, Sigma-Aldrich). Then, FT-IR spectra were recorded every 10 °C with increasing the cell temperature at a ramp rate of 2.5 °C min^{-1}. Water adsorption isotherms were obtained using a VSTAR water vapor sorption analyzer (Quantachrome Instruments) at 25 °C. Before measurement, zeolite samples were degassed at 300 °C for 12 h. Water adsorption property of Sn-BEA was characterized by thermal gravimetric analysis (TGA) in a thermal analyzer (SDT600, TA instrument). 20 mg of zeolite was mixed with 0.4 mL of water and stirred at 90 °C for 1 h under 1000 rpm, followed by drying at 60 °C oven for 16 h. Around 10 mg of the sample was put into the TGA instrument, and the sample temperature was then increased with a ramping rate of 10 °C min^{-1} to 700 °C while flowing helium at 100 mL min^{-1}. ^{29}Si MAS NMR measurements were performed on a Bruker 600 MHz solid state NMR spectrometer using a 4 mm MAS probe. The samples were spun at 6 kHz during the measurement, with the spectral operating frequencies at 600.1 and 119.2 MHz for ^{1}H and ^{29}Si nuclei respectively. A recycle delay time of 200 s was used for all the samples.

2.6. Catalytic evaluation

The catalytic activity of the Sn-BEA zeolites was studied for sugar isomerizations including the conversion of glucose to fructose and the conversion of lactose and lactulose in two different solvents i.e., water and methanol (MeOH, 99.9%, Fischer Scientific). For glucose isomerization in water, 1 g of 1 wt% glucose in water was mixed with Sn-BEA in a closed glass vial. The molar ratio of glucose to Sn was 20. The reaction proceeded at 100 °C for 15 min on an aluminum heating block. For glucose isomerization in MeOH, the reaction occurred at 70 °C for 15 min after 1 g of 1 wt% glucose in MeOH was mixed with Sn-BEA (a glucose/Sn molar ratio = 20). In addition, the conversion of lactose was performed in both water and MeOH, respectively. The Sn-BEA catalyst was mixed with either 1 g of 1 wt% lactose in water or 1 g of 0.5 wt% lactose in MeOH. The molar ratio of lactose to Sn in the initial reaction mixture was 20 for lactose isomerization in both solvents. The lactose reaction was carried out in water at 110 °C for 2 h, while the reaction occurred in MeOH at 90 °C for 16 h. After the reaction, the reaction mixture was cooled down in ice water and filtered by a 200 nm syringe filter. The filtrate was then analyzed on HPLC (LC029C Shimadzu) using a refractive index (RI) detector and an HPX-87C column (BioRad) at 80 °C under 0.6 mL min^{-1} of water (for HPLC, Fisher Scientific).

3. Results and discussion

Synthesis of hydrophobic Sn-BEA samples with tunable morphologies using the recrystallization method started from the dealumination of three different Al-BEA zeolites: bulky Al-BEA (Com_Al-BEA), 200 nm Al-BEA (200 nm_Al-BEA) and three-dimensionally ordered mesoporous imprinted Al-BEA (3DOm-i_Al-BEA). Sn was incorporated into the

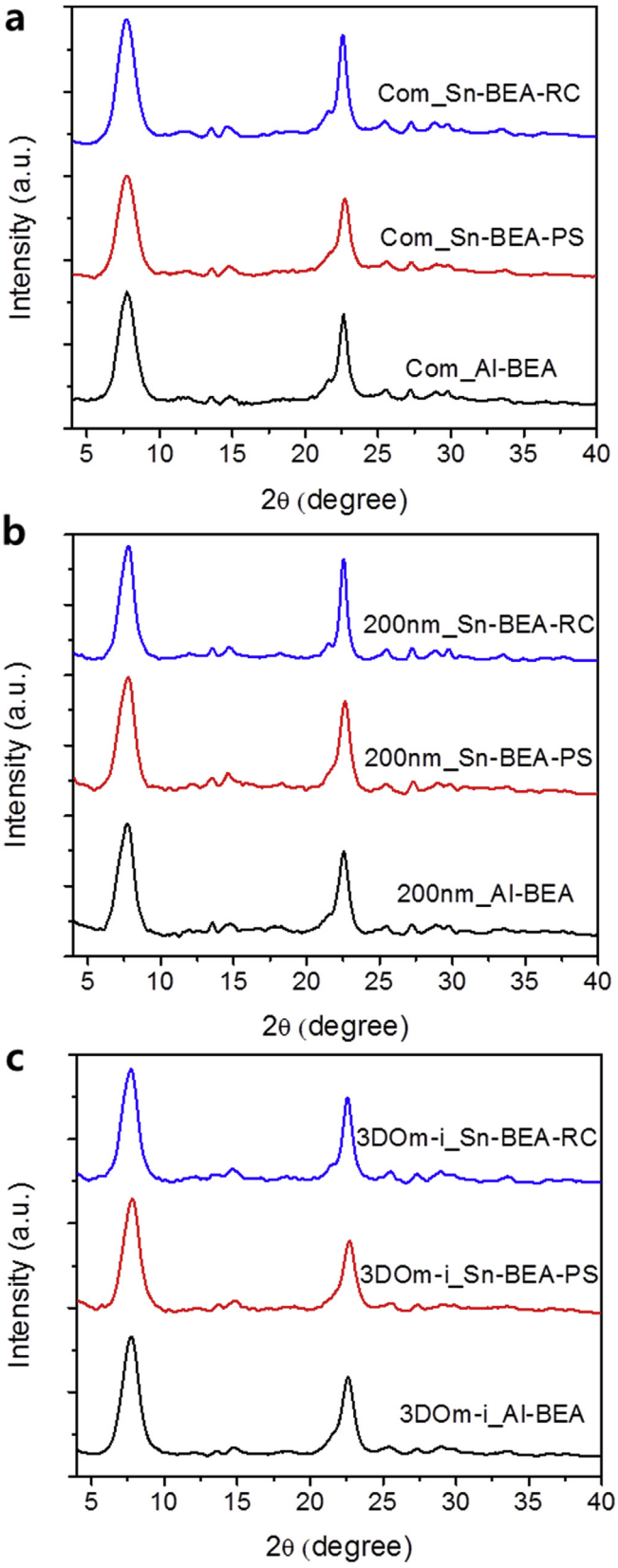

Fig. 1. XRD patterns of the parent Al-BEA, Sn-BEA made by post-synthetic method and Sn-BEA made by the recrystallization method. (a) Samples made from commercial Al-BEA: Com_Al-BEA, Com_Sn-BEA-PS and Com_Sn-BEA-RC, (b) samples made from 200 nm Al-BEA: 200 nm_Al-BEA, 200 nm_Sn-BEA-PS and 200 nm_Sn-BEA-RC, and (c) samples made from 3DOm-i Al-BEA: 3DOm-i_Al-BEA, 3DOm-i_Sn-BEA-PS and 3DOm-i_Sn-BEA-RC.

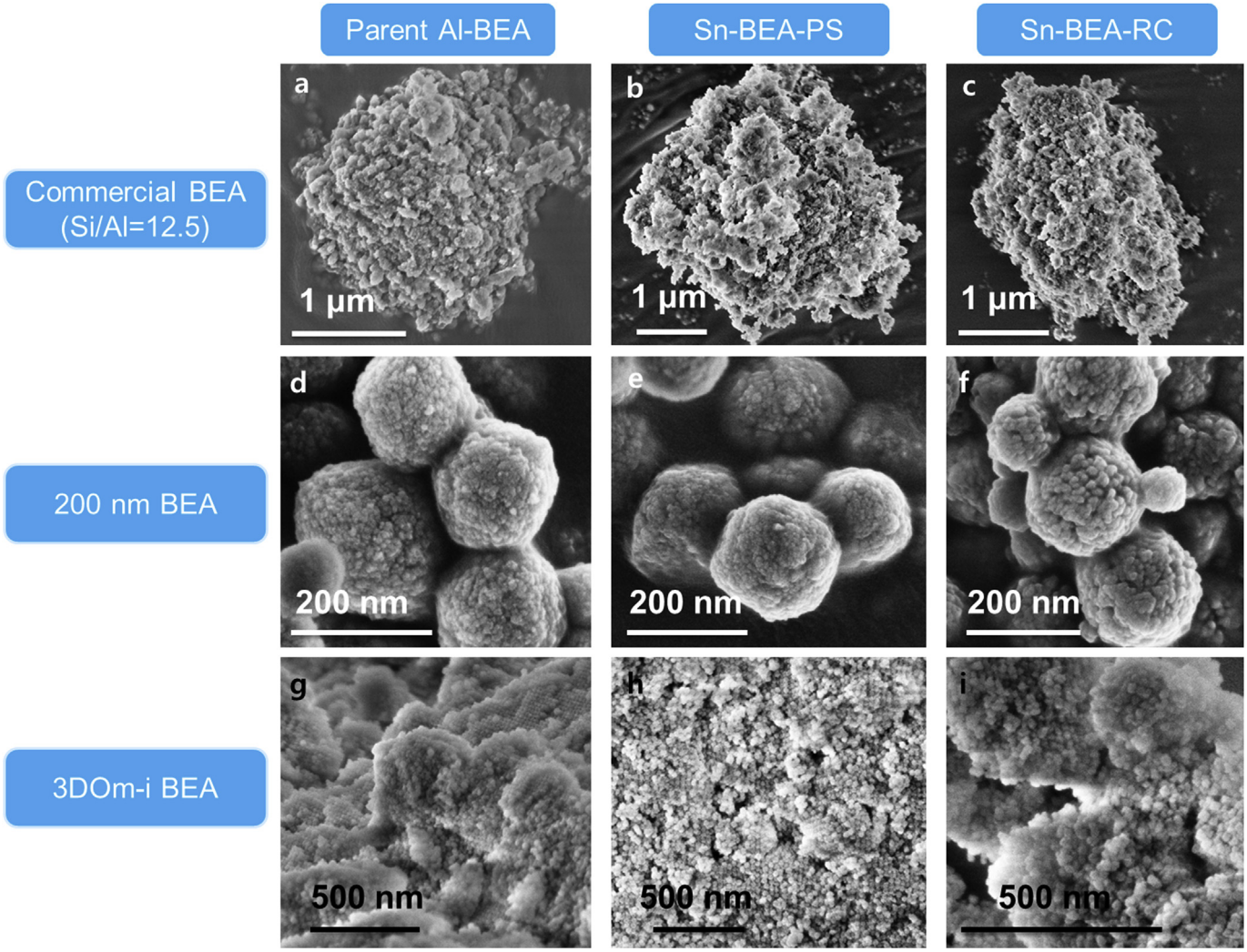

Fig. 2. SEM images of the parent Al-BEA, Sn-BEA made by post-synthetic method and Sn-BEA made by the recrystallization method. Sample made from commercial Al-BEA: (a) Com_Al-BEA, (b) Com_Sn-BEA-PS, (c) Com_Sn-BEA-RC; samples made from 200 nm Al-BEA: (d) 200 nm_Al-BEA, (e) 200 nm_Sn-BEA-PS, (f) 200 nm_Sn-BEA-RC; samples made from 3DOm-i Al-BEA: (g) 3DOm-i_Al-BEA, (h) 3DOm-i_Sn-BEA-PS, and (i) 3DOm-i_Sn-BEA-RC.

dealuminated BEA zeolites using the solid state ion-exchange (SSIE) method previously reported in literature [31]. The Sn-BEA samples prepared by the post-synthetic SSIE method are denoted as Sn-BEA-PS. In order to improve the hydrophobicity of the Sn-BEA samples while retaining their morphologies, the SAC method was applied for Sn-BEA-PS samples in the presence of TEABr and NH_4F. The final molar composition of the mixture by the SAC method was 1.00 Sn-BEA-PS: 0.54 TEABr: 0.54 NH_4F. In the experimental SAC set-up for the recrystallization, the solid mixture was placed in a glass vial with a small amount of water outside the glass vial (Fig. S1) [41,42]. The recrystallization was performed in a Teflon-lined stainless steel autoclave (50 mL capacity) at 170 °C. The samples after the recrystallization are referred to as Sn-BEA-RC. Conventional Sn-BEA was hydrothermally synthesized using HF, denoted as Sn-BEA-HF (Fig. S2a).

The XRD patterns of parent, dealuminated and recrystallized BEA zeolites are displayed in Fig. 1. All the samples show two main features at $2\theta = 7.5^\circ$ and $2\theta = 22.4^\circ$, which are the characteristics of BEA zeolites with mixed polymorphs [28,31,37]. No substantial decrease in diffraction intensity is detected for the samples after dealumination and Sn incorporation, indicating that the extraction of Al out from the framework does not cause significant change in the crystallinity. These results also suggest that recrystallization of the Sn-BEA-PS samples using TEABr and NH_4F does not form other zeolite phases. For both Sn-BEA-RC and Sn-BEA-PS, no detectable diffraction peaks of SnO_2 at $2\theta = 26.7^\circ$ and $2\theta = 34^\circ$ is observed, indicating a successful dispersion of Sn within the samples (Fig. S2b).

As displayed in Fig. 2, the three Sn-BEA-RC samples show similar morphologies to their corresponding parent Al-BEA zeolites. The parent commercial Al-BEA is an aggregate of small particles with a size of tens of nanometers. The parent 200 nm_Al-BEA synthesized using tetraethylammonium hydroxide (TEAOH) exhibits a spherical morphology composed of small sub-particles. The 3DOm-i_Al-BEA consists of an aggregation of approximately 35 nm zeolite nanocrystals assembled into an ordered mesoporous structure. During dealumination of the Al-BEA samples, subsequent Sn incorporation and recrystallization steps, no significant change in morphology is observed, indicating that the final products inherit the morphology of their parent zeolites after the recrystallization step. The Si/Sn molar ratios of all Sn-BEA-PS and Sn-BEA-RC samples are detected to be 125, according to ICP analysis. This is indicative of no leaching of Sn atoms occurred during the recrystallization step. The porous structure of BEA is well retained after the recrystallization process, evidenced by no difference in micropore volume between the three Sn-BEA-RC samples and the corresponding Sn-BEA-PS samples (Fig. S3 and Table S1). The BET surface area of Com_Sn-BEA-RC, 200 nm_Sn-BEA-RC and 3DOm-i Sn-BEA-RC is 498 $m^2 g^{-1}$, 569 $m^2 g^{-1}$ and 637 $m^2 g^{-1}$, respectively, indicating the large external surface area for the nanocrystalline and hierarchical Sn-BEA-RC samples. Furthermore, 3DOm-i_Sn-BEA-RC exhibits a hysteresis

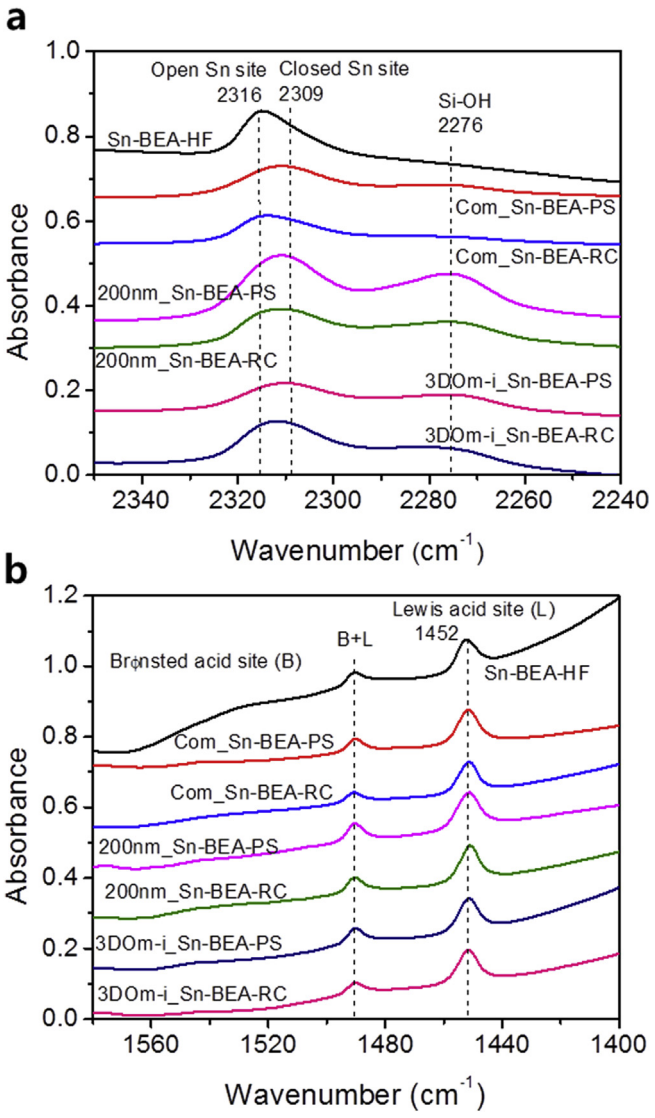

Fig. 3. FT-IR spectra of Sn-BEA-RC, Sn-BEA-PS and Sn-BEA-HF catalysts using (a) deuterated acetonitrile (CD_3CN) and (b) pyridine as probe molecules. The spectra were collected after desorbing CD_3CN at 50 °C and pyridine at 200 °C, respectively.

loop in the N_2 adsorption-desorption isotherm (Fig. S3), confirming that the mesoporous structure in 3DOm-i_Sn-BEA is retained.

The presence of the framework Sn in the Sn-BEA samples is evidenced by deuterated acetonitrile (CD_3CN) FT-IR, since this probe molecule exclusively adsorbs on the isolated, tetrahedral Lewis acidic center arising from the framework Sn [29,43]. As highlighted in Fig. 3a and Fig. S4, three main bands are visible in the spectra. The feature at 2276 cm^{-1} is assigned to the ν (C≡N) stretching mode of acetonitrile adsorbed on silanol groups (Si—OH) [5,44]. In contrast, two bands at 2309 cm^{-1} and 2316 cm^{-1} correspond to the closed Sn site (four-fold coordinated to the siliceous framework) and the open Sn site (three-fold coordinated to the zeolite framework with one Sn—OH group), respectively [22,24,29,32,45]. It is found that Sn-BEA-HF exhibits at least a 4-fold increase in the peak ratio of open Sn sites to closed Sn sites as compared with Sn-BEA-PS (Fig. 3a, S4 and S5, and Table 1). This observation is in good agreement with previous reports [24,30,44,46]. As listed in Table 1, the Sn-BEA-RC samples have higher peak ratios of open Sn sites to closed Sn sites than the Sn-BEA-PS samples by factors from 2.2 to 2.8, suggesting that the recrystallization method is able to change Sn site environment, favoring the formation of open Sn sites. Several efforts have been made so far to investigate the nature of active Lewis acid sites on Sn-BEA. It was suggested that open Sn sites are the dominant active sites for the BV reactions [7,47] and glucose isomerization [45,48,49]. On the other hand, it was proposed that closed Sn sites are catalytically active sites in the MPV transfer hydrogenation of 5-hydroxymethylfurfural and various ketones [46,50]. Therefore, synthesizing Sn-BEA catalysts with tailorable ratios of open and closed Sn sites is vital in controlling their catalytic property. The results reported here suggest that the ratio of open and closed Sn sites might be redistributed during the recrystallization process.

The Lewis acidity of the Sn-BEA samples is further confirmed by FT-IR using pyridine as a probe molecule. Unlike CD_3CN, pyridine is used as a base titrant of Lewis acid sites, which does not distinguish open and closed Lewis acid Sn sites [8,14,45]. As shown in Fig. 3b and Fig. S6, the Sn-BEA-RC samples exhibit a strong absorption at 1452 cm^{-1}, pointing to pyridine molecules bound with the Lewis acidic Sn sites [51,52]. No significant absorption signal around 1545 cm^{-1} associated with the Brønsted acid is observed in the spectra [51,52]. All these characterization results suggest that the three Sn-BEA-RC samples provide mainly framework coordinated Sn atoms, which are responsible for the Lewis acidity of the Sn-BEA samples.

In order to understand the Sn insertion and the hydrophobicity of the formed Sn-BEA samples, the silanol defects in the Sn-BEA samples before and after the recrystallization step are characterized by FT-IR. In Fig. 4, the two bands at 3745 cm^{-1} and 3735 cm^{-1} are assigned to the silanol groups on the external surface and inside the micropores of zeolites, respectively [53,54]. The band around 3500 cm^{-1} corresponds to the silanol nests [53]. The FT-IR results show that the recrystallization route leads to significant reduction in the silanol nests of all three Sn-BEA-RC samples. The reduction in the silanol defects might be due to the role of fluoride as a mineralizing agent which can restructure the silanol nests into fully coordinated silica structure. Interestingly, the restructuring process requires the presence of TEA^+, since the sole use of NH_4F in the recrystallization results in complete collapse of the BEA framework (Fig. S7). The essential role of TEA^+ is also supported by the thermogravimetric analysis (TGA) as shown in Fig. S8 and Table S2, which reveals that TEA^+ is included in the as-made Sn-BEA-RC samples. These findings suggest that restructuring of the silanol nests during the recrystallization step might be a concerted process with TEA^+ and NH_4F via dissolution and recrystallization of the silica framework.

The effect of recrystallization time on the formation of Com_Sn-BEA-RC from Com_Sn-BEA-PS is investigated. The XRD patterns of Com_Sn-BEA-RC synthesized for long recrystallization times (4 and 7 days) show a relatively low intensity for the XRD peak at $2\theta = 7.5°$, compared with the peak at $2\theta = 22.4°$ (Fig. S7 and Table S3). This is indicative of the partial collapse of BEA structure with the long recrystallization time. The TGA of the samples with varying the recrystallization time suggests that the OSDA occluded in the as-made Com_Sn-BEA-RC samples

Table 1
Peak ratio of open Sn sites to closed Sn sites in CD_3CN FT-IR spectra.

Peak ratio[a]	Sn-BEA-HF	Com_Sn-BEA-PS	Com_Sn-BEA-RC	200 nm_Sn-BEA-PS	200 nm_Sn-BEA-RC	3DOm-i_Sn-BEA-PS	3DOm-i_Sn-BEA-RC
Open Sn/Closed Sn	1.67	0.39	0.91	0.39	0.85	0.33	0.92

[a] Peak ratio of open Sn sites to closed Sn sites was obtained from peak deconvolution as shown in Fig. S5 and molar extinction coefficients of 1.04 cm μmol^{-1} and 2.04 cm μmol^{-1} for open Sn sites at 2316 cm^{-1} and closed Sn sites at 2309 cm^{-1}, respectively [45].

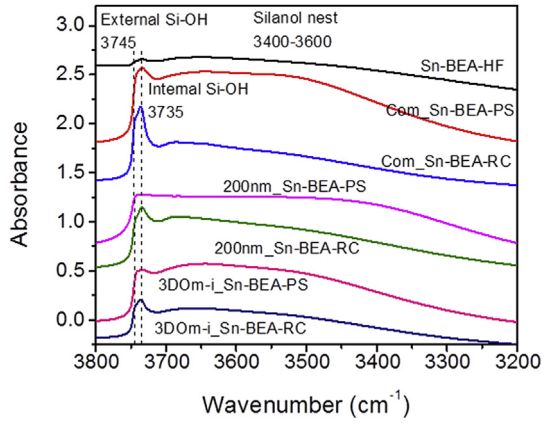

Fig. 4. FT-IR spectra in the OH-stretch region ($3800-3000\,cm^{-1}$) of the Sn-BEA samples.

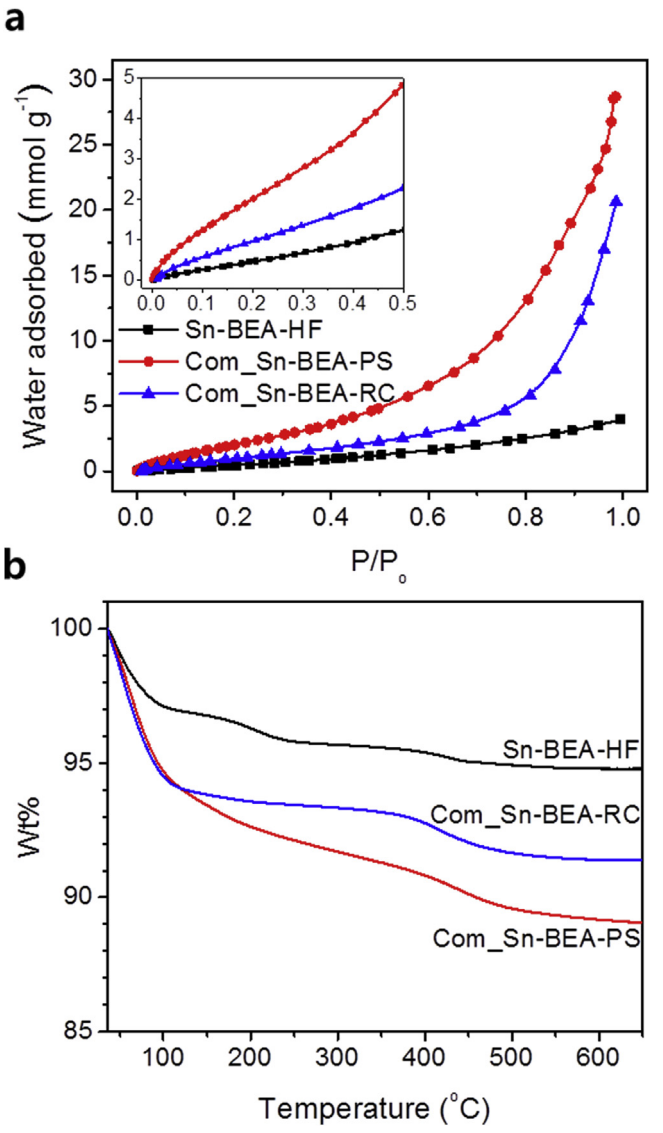

Fig. 5. (a) Water vapor adsorption isotherms at 25 °C and (b) thermogravimetric analysis (TGA) of water adsorption on Sn-BEA-HF, Com_Sn-BEA-PS and Com_Sn-BEA-RC zeolites. Prior to TGA, 20 mg of samples was mixed with 0.4 mL of water and stirred at 90 °C for 1 h under 1000 rpm, followed by drying at 60 °C oven for 16 h.

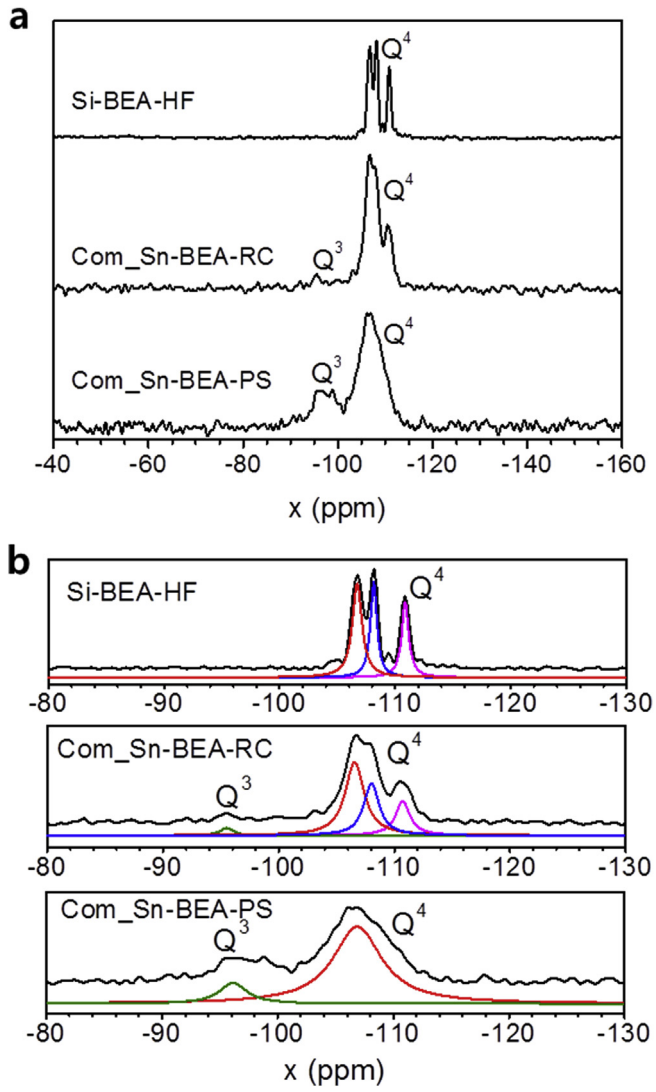

Fig. 6. ^{29}Si MAS NMR spectra of (a) Com_Sn-BEA-PS, Com_Sn-BEA-RC and Si-BEA-HF and (b) the corresponding peak deconvolution for their spectra.

decreases from 16.5 wt% to 13.1 wt% (Fig. S8 and Table S2). The OSDA located inside the as-made highly crystalline Sn-BEA-HF is 16.8 wt%. Thus, we speculate that the decomposition of TEA molecules at 170 °C contributes to the loss of crystallinity of Com_Sn-BEA-RC samples when the crystallization time is longer than 2 days.

To understand the hydrophobic property of the Sn-BEA samples, water vapor adsorption isotherms of Com_Sn-BEA-RC and Com_Sn-BEA-PS samples were collected at 25 °C and compared with that of Sn-BEA-HF. As displayed in Fig. 5a, Sn-BEA-HF reveals a lower water uptake, and in turn a higher degree of hydrophobicity, in the entire range of relative pressure (P/P_o) than Com_Sn-BEA-RC and Com_Sn-BEA-PS samples. This is explained by the low defect density of three types of silanol groups (internal and external groups, and silanol nest) in Sn-BEA-HF, as shown in Fig. 4. Com_Sn-BEA-RC exhibits a lower water uptake in comparison with Com_Sn-BEA-PS, indicating that the re-crystallization method does increase the hydrophobicity of the Sn-BEA samples, which might be attributed to the reduced number of structural defects [17,55].

TGA was also employed to characterize the hydrophobicity of the Sn-BEA samples. Water-treated Sn-BEA zeolites were prepared by mixing 20 mg of Sn-BEA samples with 0.4 mL of water at 90 °C for 1 h, followed by drying at 60 °C for 16 h. Upon heating the water-treated Sn-BEA samples, weakly bound physisorbed water desorbs below 100 °C

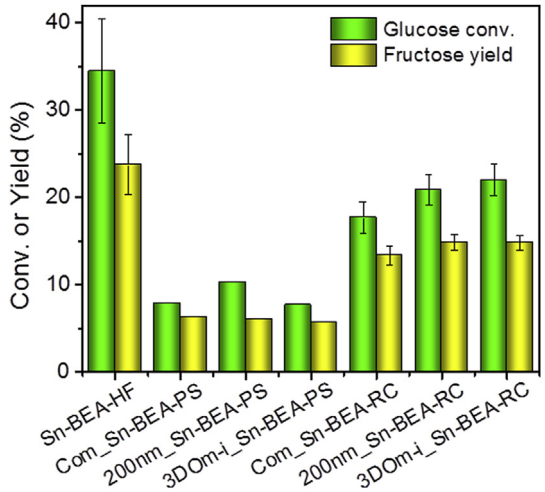

Fig. 7. Initial catalytic activities of Sn-BEA-HF, Sn-BEA-PS and Sn-BEA-RC catalysts for aqueous isomerization of glucose. Reaction conditions are as follows: initial glucose concentration of 1 wt%; a glucose to Sn molar ratio of 20; 100 °C at 15 min.

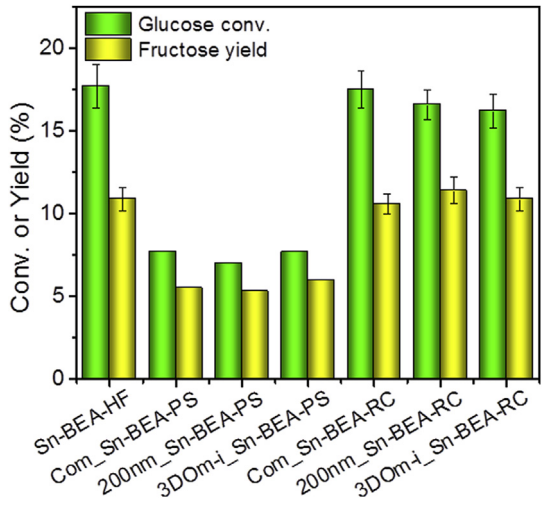

Fig. 8. Initial catalytic activities of Sn-BEA-HF, Sn-BEA-PS and Sn-BEA-RC catalysts for glucose isomerization in MeOH. Reaction conditions are as follows: initial glucose concentration of 1 wt%; a glucose to Sn molar ratio of 20; 70 °C at 15 min.

(Fig. 5b), while strongly hydrogen-bonded water is gradually released from the samples in the temperature range from ~110 °C to ~400 °C [56–58]. The weight loss of Sn-BEA-HF is lower than that of Com_Sn-BEA-RC and Com_Sn-BEA-PS, which is caused by the hydrophobic nature of Sn-BEA-HF via the fluoride-assisted synthetic route. Com_Sn-BEA-RC releases a lower amount of water than Com_Sn-BEA-PS in the temperature range from ~110 °C to ~400 °C, suggesting no strongly hydrogen-bonded water in Com_Sn-BEA-RC. This is attributable to the reduced silanol defects in Com_Sn-BEA-RC [59]. Com_Sn-BEA-RC and Com_Sn-BEA-PS show weight loss above ~400 °C accounting for 1–3 wt % of the samples, which is associated with the condensation of silanol groups at an onset temperature between 400 °C and 700 °C [56–58]. Therefore, it can be concluded that the recrystallization method indeed improve the hydrophobicity of the Sn-BEA samples. However, it is not possible to eliminate all silanol defects by this method and make the samples have the same number of defects as Sn-BEA-HF, which agrees well with the FT-IR results (Fig. 4).

^{29}Si MAS NMR results of Si-BEA-HF, Com_Sn-BEA-PS and Com_Sn-BEA-RC samples are shown in Fig. 6. Com_Sn-BEA-PS reveals a broad Q^4 ($Si(OSi)_4$) peak at −107 ppm, and a broad Q^3 ($SiOH(OSi)_3$) peak centered at −97 ppm [60,61]. In contrast, Com_Sn-BEA-RC exhibits two distinct Q^4 peaks and a much smaller Q^3 peak. This demonstrates that the recrystallization process greatly reduced the silanol groups in Com_Sn-BEA-PS, presumably making Com_Sn-BEA-RC more hydrophobic in nature due to fewer defects in the samples. The ^{29}Si MAS NMR spectrum of the reference sample Si-BEA-HF has three highly distinct Q^4 peaks without a noticeable Q^3 peak, indicating a highly crystalline sample with crystallographically distinct T-sites [38,62]. The chemical shifts of the Q^4 peaks of Si-BEA-HF match well with the chemical shifts of the Q^4 peaks of Com_Sn-BEA-RC obtained from peak deconvolution (Fig. 6b). A comparison of the ^{29}Si MAS NMR spectra between Com_Sn-BEA-PS and Com_Sn-BEA-RC shows two major differences: Com_Sn-BEA-RC possesses narrow and distinct Q^4 peaks with a small Q^3 peak (Fraction of Q^3 peak area, i.e., $Q^3/(Q^3+Q^4) = 0.04$), whereas Com_Sn-BEA-PS shows a wide Q^4 peak and significantly more Q^3 contribution (Fraction of Q^3 peak area, i.e., $Q^3/(Q^3+Q^4) = 0.18$). This NMR study indicates that the recrystallization process can reduce the number of silanol defects.

The studies on the recrystallization step using XRD, SEM, FT-IR and NMR suggest that the partial dissolution and restructuring of the silanol defects of Sn-BEA-PS occur locally within the samples. The observation of retaining the original morphology of parent zeolites is in contrast to earlier reports where dramatic morphological changes of parent zeolites were observed during a similar recrystallization process [63–73]. Hollow MFI crystals such as silicalite-1, ZSM-5 and TS-1 were synthesized by recrystallizing conventional coffin-like MFI zeolites with tetrapropylammonium hydroxide (TPAOH) [64–68]. A hollow morphology of SAPO-34 with CHA topology was obtained using TEAOH

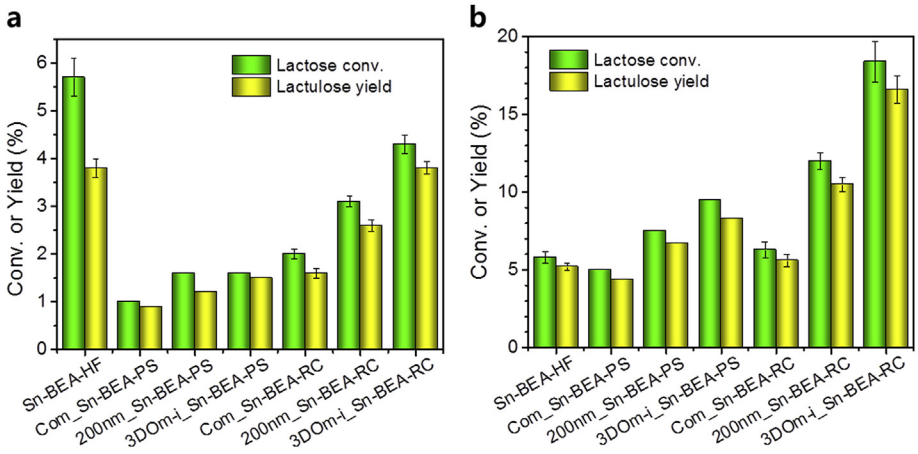

Fig. 9. Initial catalytic activities of Sn-BEA-HF, Sn-BEA-PS and Sn-BEA-RC catalysts for lactose isomerization in (a) water and (b) MeOH, respectively. Reaction conditions are as follows: initial lactose concentration of 1 wt% and 0.5 wt% in water and MeOH, respectively; a substrate to Sn molar ratio of 20; 110 °C at 2 h (in water), and 90 °C at 16 h (in MeOH).

[63]. By tailoring recrystallization parameters, mesoporous zeolites were also synthesized from conventional ones by the recrystallization method [69–73]. The morphological difference between the parent zeolites and the recrystallized zeolites is presumably controlled by the recrystallization kinetics which entails the partial dissolution of zeolite frameworks, the formation of zeolite precursors and their growth on the surface of the parent zeolites. During the recrystallization process for making the Sn-BEA-RC samples, the dissolution rate is likely similar to the restructuring rate of the silanol defects. If the former is much faster than the latter, the morphology of recrystallized zeolites would be noticeably different from that of the parent zeolites. In addition, the steam-assisted recrystallization conditions employed in this recrystallization process may also contribute to retain the morphology of the Sn-BEA-RC samples from the parent Sn-BEA samples, because only limited amount of water can participate in the recrystallization through vapor phase at 170 °C in the SAC experimental set-up. The highly dense synthesis mixture could limit the mass transport of the solid and hinder the event of new nucleation as well as substantial morphology change.

Glucose isomerization in water is used to study the catalytic property of Sn-BEA-RC, Sn-BEA-PS and Sn-BEA-HF samples. It is generally known that glucose undergoes isomerization to generate fructose via an intramolecular 1,2 hydride shift reaction over Sn containing zeolite catalysts [19]. As shown in Fig. 7, under identical conditions Sn-BEA-HF produces a fructose yield of 23.7%, whereas the three Sn-BEA-PS catalysts show a similar fructose yield of 6.1%, revealing that the Sn-BEA catalysts prepared through the post-synthetic route are less active than the hydrophobic Sn-BEA-HF. This result is consistent with previous literature [17,74], confirming that the hydrophilic environment arising from highly defective surface is detrimental for the catalytic activity of Sn-BEA catalysts. Notably, three Sn-BEA-RC catalysts display a fructose yield of ~14.8%, which is 2.5 times higher than three Sn-BEA-PS samples, but still lower than Sn-BEA-HF. This is evident that Sn-BEA-RC catalysts are more active than Sn-BEA-PS catalysts, presumably due to the lower density of silanol defects in Sn-BEA-RC samples and different Sn site structures (Figs. 4 and 6). Regardless of the morphology of Sn-BEA-RC samples, comparable catalytic activities are detected. These observations are also found from three Sn-BEA-PS catalysts. This result suggests that diffusion limitation is not a major factor for the isomerization of glucose over Sn-BEA catalysts under these reaction conditions.

To gain further insights into the effects of surface properties of the Sn-BEA catalysts on their catalytic property, MeOH is chosen as a solvent for glucose isomerization. Interestingly, the three Sn-BEA-RC catalysts produce comparable product yields to Sn-BEA-HF, which display much higher catalytic performances than the Sn-BEA-PS catalysts (Fig. 8). These results suggest that the difference in hydrophobicity between Sn-BEA-RC and Sn-BEA-HF is not critical for the glucose isomerization in MeOH. The effect from the solvent is not fully understood yet. This might be due to the different dielectric constants of MeOH and water, and MeOH favors physical interaction with non-polar siloxane bonds (Si—O—Si) of the Sn-BEA-RC and Sn-BEA-HF catalysts [17,55,75–77]. In addition, this observation might also be ascribed to different MeOH adsorption properties to the Sn sites of the Sn-BEA samples [17,74,75].

Furthermore, catalytic activities of the Sn-BEA-RC catalysts for bulky lactose isomerization are explored, and compared with those of the Sn-BEA-PS and Sn-BEA-HF catalysts. Lactose is a sugar dimer built of galactose and glucose units linked via a β (1–4) glycosidic bond (Fig. S9), which serves as a precursor for sugar derivatives such as sugar acids and sugar alcohols in food and pharmaceutical industries [78]. Previous studies have shown that Sn-BEA zeolites catalyze the isomerization of lactose into lactulose [36,78,79]. In aqueous lactose isomerization, the three Sn-BEA-PS catalysts show lactulose yield in the following order: 3DOm-i_Sn-BEA-PS > 200 nm_Sn-BEA-PS > Com_Sn-BEA-PS (Fig. 9a). This result indicates that the small particle size and hierarchical structure might facilitate the access of lactose to the active sites, resulting in their enhanced catalytic properties. This observation is different from the aqueous glucose isomerization where these three catalysts exhibit similar catalytic performance. It is likely that diffusion limitation in the Sn-BEA catalysts becomes crucial for the aqueous lactose isomerization owing to the bulky size of lactose compared to glucose. More importantly, the recrystallization of the Sn-BEA-PS further improves the catalytic property for the Sn-BEA samples. The three Sn-BEA-RC catalysts produce higher lactulose yields than their corresponding Sn-BEA-PS catalysts by a factor of 1.8–2.5, which confirms the key role of the hydrophobicity of Sn-BEA catalysts for the bulky sugar isomerization in water. Notably, Sn-BEA-HF and 3DOm-i_Sn-BEA-RC samples catalyze the lactose isomerization to a similar extent although the particle size of former is much larger than the domain size of the latter. This suggests the catalytic property of Sn-BEA catalysts for the isomerization of lactose is regulated by both the hydrophobicity and the mass transport property of the catalysts. Hierarchical 3DOm-i_Sn-BEA-RC provides improved mass transport for the reaction, however, its hydrophobicity is still lower than that of Sn-BEA-HF. Interestingly, when switching solvent from water to MeOH, 3DOm-i_Sn-BEA-RC achieves 3.2 times higher reaction rate than Sn-BEA-HF (Fig. 9b). In this case, the hydrophobicity of the Sn-BEA catalysts appears less crucial for the isomerization of lactose in MeOH. The enhanced product yields on 3DOm-i_Sn-BEA-RC can be interpreted by the reduced diffusion limitation of lactose within the hierarchically structured catalyst.

4. Conclusions

Hydrophobic Sn-BEA zeolites with different morphologies were successfully synthesized by the recrystallization of highly defective Sn-BEA samples (Sn-BEA-PS) using NH_4F and TEABr. During the recrystallization step, the defects of Sn-BEA-PS samples are reduced, likely due to the rearrangement of the defects within the samples. The reduced density of silanol defects mitigates the interaction between the catalysts and water, rendering Sn-BEA-RC samples more hydrophobic than Sn-BEA-PS samples. The Sn-BEA samples fabricated by the recrystallization method inherit the morphology of their parent Al-BEA samples, thereby providing a versatile approach to control the morphology of Sn-BEA. The nanocrystalline and hierarchical Sn-BEA catalysts by the recrystallization method are superior for the reactions involving bulky molecules because of the improved hydrophobicity and mass transport property. The recrystallization method is a simple and reliable strategy to enhance the hydrophobic property of Sn-BEA catalysts with tailored morphologies.

Acknowledgements

This work was supported by the Catalysis Center for Energy Innovation, an Energy Frontier Research Center funded by the US Dept. of Energy, Office of Science, and Office of Basic Energy Sciences under award number DE-SC0001004.

Appendix A. Supplementary data

Supplementary data to this article can be found online at https://doi.org/10.1016/j.micromeso.2018.12.046.

References

[1] M.E. Davis, Ordered porous materials for emerging applications, Nature 417 (2002) 813–821.
[2] A. Corma, From microporous to mesoporous molecular sieve materials and their use in catalysis, Chem. Rev. 97 (1997) 2373–2419.
[3] M. Boronat, A. Corma, M. Renz, P.M. Viruela, Predicting the activity of single isolated Lewis acid sites in solid catalysts, Chem. Eur J. 12 (2006) 7067–7077.
[4] A. Corma, L.T. Nemeth, M. Renz, S. Valencia, Sn-zeolite beta as a heterogeneous chemoselective catalyst for Baeyer-Villiger oxidations, Nature 412 (2001) 423–425.
[5] M. Boronat, P. Concepcion, A. Corma, M. Renz, S. Valencia, Determination of the catalytically active oxidation Lewis acid sites in Sn-beta zeolites, and their

optimisation by the combination of theoretical and experimental studies, J. Catal. 234 (2005) 111–118.
[6] A. Corma, M.E. Domine, L. Nemeth, S. Valencia, AI-free Sn-beta zeolite as a catalyst for the selective reduction of carbonyl compounds (Meerwein-Ponndorf-Verley reaction), J. Am. Chem. Soc. 124 (2002) 3194–3195.
[7] M. Boronat, A. Corma, M. Renz, Mechanism of the Meerwein-Ponndorf-Verley-Oppenauer (MPVO) redox equilibrium on Sn- and Zr-beta zeolite catalysts, J. Phys. Chem. B 110 (2006) 21168–21174.
[8] B. Tang, W.L. Dai, G.J. Wu, N.J. Guan, L.D. Li, M. Hunger, Improved postsynthesis strategy to Sn-beta zeolites as Lewis acid catalysts for the ring-opening hydration of epoxides, ACS Catal. 4 (2014) 2801–2810.
[9] C.C. Chang, H.J. Cho, J.Y. Yu, R.J. Gorte, J. Gulbinski, P. Dauenhauer, W. Fan, Lewis acid zeolites for tandem Diels-Alder cycloaddition and dehydration of biomass-derived dimethylfuran and ethylene to renewable p-xylene, Green Chem. 18 (2016) 1368–1376.
[10] C.C. Chang, S.K. Green, C.L. Williams, P.J. Dauenhauer, W. Fan, Ultra-selective cycloaddition of dimethylfuran for renewable p-xylene with H-BEA, Green Chem. 16 (2014) 585–588.
[11] J.J. Pacheco, M.E. Davis, Synthesis of terephthalic acid via Diels-Alder reactions with ethylene and oxidized variants of 5-hydroxymethylfurfural, Proc. Natl. Acad. Sci. U.S.A. 111 (2014) 8363–8367.
[12] J.J. Pacheco, J.A. Labinger, A.L. Sessions, M.E. Davis, Route to renewable PET: reaction pathways and energetics of diels-alder and dehydrative aromatization reactions between ethylene and biomass-derived furans catalyzed by Lewis acid molecular sieves, ACS Catal. 5 (2015) 5904–5913.
[13] C.L. Williams, C.C. Chang, P. Do, N. Nikbin, S. Caratzoulas, D.G. Vlachos, R.F. Lobo, W. Fan, P.J. Dauenhauer, Cycloaddition of biomass-derived furans for catalytic production of renewable p-xylene, ACS Catal. 2 (2012) 935–939.
[14] J. Yu, S. Zhu, P.J. Dauenhauer, H.J. Cho, W. Fan, R.J. Gorte, Adsorption and reaction properties of SnBEA, ZrBEA and H-BEA for the formation of p-xylene from DMF and ethylene, Catal. Sci. & Technol. 6 (2016) 5729–5736.
[15] H.J. Cho, L. Ren, V. Vattipalli, Y.-H. Yeo, N. Gould, B. Xu, R.J. Gorte, R. Lobo, P.J. Dauenhauer, M. Tsapatsis, W. Fan, Renewable p-xylene from 2,5-dimethylfuran and ethylene using phosphorus-containing zeolite catalysts, ChemCatChem 9 (2017) 398–402.
[16] V. Choudhary, A.B. Pinar, S.I. Sandler, D.G. Vlachos, R.F. Lobo, Xylose isomerization to xylulose and its dehydration to furfural in aqueous media, ACS Catal. 1 (2011) 1724–1728.
[17] R. Gounder, M.E. Davis, Beyond shape selective catalysis with zeolites: hydrophobic void spaces in zeolites enable catalysis in liquid water, AIChE J. 59 (2013) 3349–3358.
[18] C.M. Lew, N. Rajabbeigi, M. Tsapatsis, Tin-containing zeolite for the isomerization of cellulosic sugars, Microporous Mesoporous Mater. 153 (2012) 55–58.
[19] M. Moliner, Y. Roman-Leshkov, M.E. Davis, Tin-containing zeolites are highly active catalysts for the isomerization of glucose in water, Proc. Natl. Acad. Sci. U.S.A. 107 (2010) 6164–6168.
[20] Y. Roman-Leshkov, M. Moliner, J.A. Labinger, M.E. Davis, Mechanism of glucose isomerization using a solid Lewis acid catalyst in water, Angew. Chem. Int. Ed. 49 (2010) 8954–8957.
[21] H.J. Cho, C.C. Chang, W. Fan, Base free, one-pot synthesis of lactic acid from glycerol using a bifunctional Pt/Sn-MFI catalyst, Green Chem. 16 (2014) 3428–3433.
[22] H.J. Cho, P. Dornath, W. Fan, Synthesis of hierarchical Sn-MFI as Lewis acid catalysts for isomerization of cellulosic sugars, ACS Catal. 4 (2014) 2029–2037.
[23] M.S. Holm, S. Saravanamurugan, E. Taarning, Conversion of sugars to lactic acid derivatives using heterogeneous zeotype catalysts, Science 328 (2010) 602–605.
[24] C.M. Osmundsen, M.S. Holm, S. Dahl, E. Taarning, Tin-containing silicates: structure-activity relations, Proc. Roy. Soc. a-Math. Phy. 468 (2012) 2000–2016.
[25] E. Taarning, S. Saravanamurugan, M.S. Holm, J.M. Xiong, R.M. West, C.H. Christensen, Zeolite-catalyzed isomerization of triose sugars, ChemSusChem 2 (2009) 625–627.
[26] N. Rajabbeigi, A.I. Torres, C.M. Lew, B. Elyassi, L.M. Ren, Z.P. Wang, H.J. Cho, W. Fan, P. Daoutidis, M. Tsapatsis, On the kinetics of the isomerization of glucose to fructose using Sn-Beta, Chem. Eng. Sci. 116 (2014) 235–242.
[27] C.S. Cundy, P.A. Cox, The hydrothermal synthesis of zeolites: precursors, intermediates and reaction mechanism, Microporous Mesoporous Mater. 82 (2005) 1–78.
[28] S. Tolborg, A. Katerinopoulou, D.D. Falcone, I. Sadaba, C.M. Osmundsen, R.J. Davis, E. Taarning, P. Fristrup, M.S. Holm, Incorporation of tin affects crystallization, morphology, and crystal composition of Sn-Beta, J. Mater. Chem. A 2 (2014) 20252–20262.
[29] C.C. Chang, H.J. Cho, Z.P. Wang, X.T. Wang, W. Fan, Fluoride-free synthesis of a Sn-BEA catalyst by dry gel conversion, Green Chem. 17 (2015) 2943–2951.
[30] J. Dijkmans, J. Demol, K. Houthoofd, S.G. Huang, Y. Pontikes, B. Sels, Post-synthesis Sn beta: an exploration of synthesis parameters and catalysis, J. Catal. 330 (2015) 545–557.
[31] C. Hammond, S. Conrad, I. Hermans, Simple and scalable preparation of highly active Lewis acidic Sn-beta, Angew. Chem. Int. Ed. 51 (2012) 11736–11739.
[32] C. Hammond, D. Padovan, A. Al-Nayili, P.P. Wells, E.K. Gibson, N. Dimitratos, Identification of active and spectator Sn sites in Sn-beta following solid-state stannation, and consequences for Lewis acid catalysis, ChemCatChem 7 (2015) 3322–3331.
[33] P. Li, G.Q. Liu, H.H. Wu, Y.M. Liu, J.G. Jiang, P. Wu, Postsynthesis and selective oxidation properties of nanosized Sn-beta zeolite, J. Phys. Chem. C 115 (2011) 3663–3670.
[34] J. Dijkmans, M. Dusselier, W. Janssens, M. Trekels, A. Vantomme, E. Breynaert, C. Kirschhock, B.F. Sels, An inner-/outer-sphere stabilized Sn active site in beta-zeolite: spectroscopic evidence and kinetic consequences, ACS Catal. 6 (2016) 31–46.
[35] J. Dijkmans, D. Gabriels, M. Dusselier, F. de Clippel, P. Vanelderen, K. Houthoofd, A. Malfliet, Y. Pontikes, B.F. Sels, Productive sugar isomerization with highly active Sn in dealuminated beta zeolites, Green Chem. 15 (2013) 2777–2785.
[36] R. Gounder, M.E. Davis, Monosaccharide and disaccharide isomerization over Lewis acid sites in hydrophobic and hydrophilic molecular sieves, J. Catal. 308 (2013) 176–188.
[37] C.C. Chang, Z.P. Wang, P. Dornath, H.J. Cho, W. Fan, Rapid synthesis of Sn-Beta for the isomerization of cellulosic sugars, RSC Adv. 2 (2012) 10475–10477.
[38] M.Q. Tong, D.L. Zhang, W.B. Fan, J. Xu, L.K. Zhu, W. Guo, W.F. Yan, J.H. Yu, S.L. Qiu, J.G. Wang, F. Deng, R.R. Xu, Synthesis of chiral polymorph A-enriched zeolite Beta with an extremely concentrated fluoride route, Sci Rep-Uk 5 (2015).
[39] S. Mintova, V. Valtchev, T. Onfroy, C. Marichal, H. Knozinger, T. Bein, Variation of the Si/Al ratio in nanosized zeolite Beta crystals, Microporous Mesoporous Mater. 90 (2006) 237–245.
[40] H.Y. Chen, J. Wydra, X.Y. Zhang, P.S. Lee, Z.P. Wang, W. Fan, M. Tsapatsis, Hydrothermal synthesis of zeolites with three-dimensionally ordered mesoporous-imprinted structure, J. Am. Chem. Soc. 133 (2011) 12390–12393.
[41] P.R.H.P. Rao, K. Ueyama, M. Matsukata, Crystallization of high silica BEA by dry gel conversion, Appl. Catal. A 166 (1998) 97–103.
[42] W. Fan, M.A. Snyder, S. Kumar, P.S. Lee, W.C. Yoo, A.V. McCormick, R.L. Penn, A. Stein, M. Tsapatsis, Hierarchical nanofabrication of microporous crystals with ordered mesoporosity, Nat. Mater. 7 (2008) 984–991.
[43] S. Roy, K. Bakhmutsky, E. Mahmoud, R.F. Lobo, R.J. Gorte, Probing Lewis acid sites in Sn-beta zeolite, ACS Catal. 3 (2013) 573–580.
[44] M. Boronat, P. Concepcion, A. Corma, M.T. Navarro, M. Renz, S. Valencia, Reactivity in the confined spaces of zeolites: the interplay between spectroscopy and theory to develop structure-activity relationships for catalysis, Phys. Chem. Chem. Phys. 11 (2009) 2876–2884.
[45] J.W. Harris, M.J. Cordon, J.R. Di Iorio, J.C. Vega-Vila, F.H. Ribeiro, R. Gounder, Titration and quantification of open and closed Lewis acid sites in Sn-Beta zeolites that catalyze glucose isomerization, J. Catal. 335 (2016) 141–154.
[46] A. Al-Nayili, K. Yakabi, C. Hammond, Hierarchically porous BEA stannosilicates as unique catalysts for bulky ketone conversion and continuous operation, J. Mater. Chem. A 4 (2016) 1373–1382.
[47] M. Boronat, A. Corma, M. Renz, G. Sastre, P.M. Viruela, A multisite molecular mechanism for Baeyer-Villiger oxidations on solid catalysts using environmentally friendly H2O2 as oxidant, Chem. Eur J. 11 (2005) 6905–6915.
[48] R. Bermejo-Deval, R. Gounder, M.E. Davis, Framework and extraframework tin sites in zeolite beta react glucose differently, ACS Catal. 2 (2012) 2705–2713.
[49] R. Bermejo-Deval, M. Orazov, R. Gounder, S.J. Hwang, M.E. Davis, Active sites in Sn-beta for glucose isomerization to fructose and epimerization to mannose, ACS Catal. 4 (2014) 2288–2297.
[50] J.D. Lewis, S. Van de Vyver, A.J. Crisci, W.R. Gunther, V.K. Michaelis, R.G. Griffin, Y. Roman-Leshkov, A continuous flow strategy for the coupled transfer hydrogenation and etherification of 5-(hydroxymethyl)furfural using Lewis acid zeolites, ChemSusChem 7 (2014) 2255–2265.
[51] L. Li, C. Stroobants, K.F. Lin, P.A. Jacobs, B.F. Sels, P.P. Pescarmona, Selective conversion of trioses to lactates over Lewis acid heterogeneous catalysts, Green Chem. 13 (2011) 1175–1181.
[52] R.M. West, M.S. Holm, S. Saravanamurugan, J.M. Xiong, Z. Beversdorf, E. Taarning, C.H. Christensen, Zeolite H-USY for the production of lactic acid and methyl lactate from C-3-sugars, J. Catal. 269 (2010) 122–130.
[53] K. Barbera, F. Bonino, S. Bordiga, T.V.W. Janssens, P. Beato, Structure-deactivation relationship for ZSM-5 catalysts governed by framework defects, J. Catal. 280 (2011) 196–205.
[54] M. Trombetta, A.G. Alejandre, J.R. Solis, G. Busca, An FT-IR study of the reactivity of hydrocarbons on the acid sites of HZSM5 zeolite, Appl. Catal. A 198 (2000) 81–93.
[55] K. Zhang, R.P. Lively, J.D. Noel, M.E. Dose, B.A. McCool, R.R. Chance, W.J. Koros, Adsorption of water and ethanol in MFI-type zeolites, Langmuir 28 (2012) 8664–8673.
[56] T.D. Courtney, C.C. Chang, R.J. Gorte, R.F. Lobo, W. Fan, V. Nikolakis, Effect of water treatment on Sn-BEA zeolite: origin of 960 cm(-1) FTIR peak, Microporous Mesoporous Mater. 210 (2015) 69–76.
[57] K.R. Lange, Characterization of molecular water on silica surfaces, J. Coll. Sci. 20 (1965) 231–&.
[58] H. Naono, R. Fujiwara, M. Yagi, Determination of physisorbed and chemisorbed waters on silica-gel and porous silica glass by means of desorption isotherms of water-vapor, J. Colloid Interface Sci. 76 (1980) 74–82.
[59] S. Saliba, P. Ruch, W. Volksen, T.P. Magbitang, G. Dubois, B. Michel, Combined influence of pore size distribution and surface hydrophilicity on the water adsorption characteristics of micro- and mesoporous silica, Microporous Mesoporous Mater. 226 (2016) 221–228.
[60] H. Jon, B. Lu, Y. Oumi, K. Itabash, T. Sano, Synthesis and thermal stability of beta zeolite using ammonium fluoride, Microporous Mesoporous Mater. 89 (2006) 88–95.
[61] P. Wolf, M. Valla, F. Núñez-Zarur, A. Comas-Vives, A. Rossini, C. Firth, H. Kallas, A. Lesage, L. Emsley, C. Copéret, I. Hermans, Correlating synthetic methods, morphology, atomic-level structure, and catalytic activity of Sn-β catalysts, ACS Catal. 6 (2016) 4047–4063.
[62] M.A. Camblor, A. Corma, S. Valencia, Spontaneous nucleation and growth of pure silica zeolite-beta free of connectivity defects, Chem. Comm. (1996) 2365–2366.
[63] Y.Y. Qiao, M. Yang, B.B. Gao, L.Y. Wang, P. Tian, S.T. Xu, Z.M. Liu, Creation of hollow SAPO-34 single crystals via alkaline or acid etching, Chem. Commun. 52

(2016) 5718–5721.
[64] C.Y. Dai, A.F. Zhang, L.L. Li, K.K. Hou, F.S. Ding, J. Li, D.Y. Mu, C.S. Song, M. Liu, X.W. Guo, Synthesis of hollow nanocubes and macroporous monoliths of silicalite-1 by alkaline treatment, Chem. Mater. 25 (2013) 4197–4205.
[65] S.W. Li, A. Tuel, D. Laprune, F. Meunier, D. Farrusseng, Transition-metal nanoparticles in hollow zeolite single crystals as bifunctional and size-selective hydrogenation catalysts, Chem. Mater. 27 (2015) 276–282.
[66] Y.R. Wang, M. Lin, A. Tuel, Hollow TS-1 crystals formed via a dissolution-recrystallization process, Microporous Mesoporous Mater. 102 (2007) 80–85.
[67] Y.R. Wang, A. Tuel, Nanoporous zeolite single crystals: ZSM-5 nanoboxes with uniform intracrystalline hollow structures, Microporous Mesoporous Mater. 113 (2008) 286–295.
[68] C.Y. Dai, A.F. Zhang, M. Liu, X.W. Guo, C.S. Song, Hollow ZSM-5 with silicon-rich surface, double shells, and functionalized interior with metallic nanoparticles and carbon nanotubes, Adv. Funct. Mater. 25 (2015) 7479–7487.
[69] D. Verboekend, M. Milina, S. Mitchell, J. Perez-Ramirez, Hierarchical zeolites by desilication: occurrence and catalytic impact of recrystallization and restructuring, Cryst. Growth Des. 13 (2013) 5025–5035.
[70] W.C. Yoo, X.Y. Zhang, M. Tsapatsis, A. Stein, Synthesis of mesoporous ZSM-5 zeolites through desilication and re-assembly processes, Microporous Mesoporous Mater. 149 (2012) 147–157.
[71] D.P. Gamliel, H.J. Cho, W. Fan, J.A. Valla, On the effectiveness of tailored mesoporous MFI zeolites for biomass catalytic fast pyrolysis, Appl. Catal. A 522 (2016) 109–119.
[72] S. Abello, A. Bonilla, J. Perez-Ramirez, Mesoporous ZSM-5 zeolite catalysts prepared by desilication with organic hydroxides and comparison with NaOH leaching, Appl. Catal. A 364 (2009) 191–198.
[73] I.I. Ivanova, E.E. Knyazeva, Micro-mesoporous materials obtained by zeolite recrystallization: synthesis, characterization and catalytic applications, Chem. Soc. Rev. 42 (2013) 3671–3688.
[74] R. Gounder, Hydrophobic microporous and mesoporous oxides as Bronsted and Lewis acid catalysts for biomass conversion in liquid water, Catal. Sci. Technol. 4 (2014) 2877–2886.
[75] J.C. Vega-Vila, J.W. Harris, R. Gounder, Controlled insertion of tin atoms into zeolite framework vacancies and consequences for glucose isomerization catalysis, J. Catal. 344 (2016) 108–120.
[76] Y.C. Long, H.W. Jiang, H. Zeng, Sorbate/framework and sorbate/sorbate interaction of organics on siliceous MFI type zeolite, Langmuir 13 (1997) 4094–4101.
[77] G. Akerlof, Dielectric constants of some organic solvent-water mixtures at various temperatures, J. Am. Chem. Soc. 54 (1932) 4125–4139.
[78] N. Seki, H. Saito, Lactose as a source for lactulose and other functional lactose derivatives, Int. Dairy J. 22 (2012) 110–115.
[79] M. Aider, D. de Halleux, Isomerization of lactose and lactulose production: review, Trends Food Sci. Technol. 18 (2007) 356–364.